

RESONANT TRAPPING OF THE MOVING GROUPS G18-39 AND G21-22 IN THE GALACTIC HALO

W. J. SCHUSTER

Instituto de Astronomía, Universidad Nacional Autónoma de México, Apdo. Postal 106, 22800 Ensenada, B.C., México.

J. G. FERNÁNDEZ-TRINCADO

Departamento de Astronomía, Casilla 160-C, Universidad de Concepción, Concepción, Chile.

Instituto de Astronomía y Ciencias Planetarias, Universidad de Atacama, Copayapu 485, Copiapó, Chile.

and

Institut Utinam, CNRS UMR 6213, Université Bourgogne-Franche-Comté,

OSU THETA Franche-Comté, Observatoire de Besançon, BP 1615, 25010 Besançon Cedex, France.

E. MORENO

Instituto de Astronomía, Universidad Nacional Autónoma de México, Apdo. Postal 70-264,
Ciudad Universitaria CDMX 04510, México.

ABSTRACT

The 3D Galactic orbits of stars in the two groups G18-39 and G21-22 pertaining to the Galactic halo have been computed in a Galactic potential including a Galactic bar. The orbits have been related with the orbital structure of resonant orbits on the Galactic plane created by the bar component. We find that the majority of stars in both groups are trapped mainly by two resonant families already studied in a previous analysis. We show that the observed U–V velocity field of the stars in both groups can be naturally explained as a result of their trapping by these two resonant families, taking the angular rotation speed of the bar approximately in the interval $45\text{--}60\text{ km s}^{-1}\text{ kpc}^{-1}$. This analysis may help to understand the identification of other known star groups as the possible result of the interactions produced by resonances on stars close to resonant families. For the two groups G18-39 and G21-22 we conclude that the majority of their stars are members of the supergroups of stars in the Galaxy trapped by two resonant families generated by the Galactic bar.

Keywords: Galaxy: kinematics and dynamics — Galaxy: halo — Galaxy: solar neighborhood

1. INTRODUCTION

[Eggen \(1958a\)](#) began a systematic study of moving groups in our Galaxy using the convergent-point method to compile stars of the young disk population in the solar neighborhood with space motions similar to the Hyades cluster and the Sirius group, and looked for the associated expected clumping of stars in the U–V velocity plane ([Eggen 1958b](#)). He found later that the Hyades and Sirius moving groups are more extended localized groups which he called superclusters ([Eggen 1983a,b](#)), in which the star members have parallel space motions and possibly come from the disruption of compact stellar clusters. As the Galactic perturbations on the clusters act over an increasing time, the star orbits distribute along a tube of orbits; he called the resulting distribution of stars a stellar group ([Eggen 1996](#)). For the old disk population [Eggen \(1991\)](#) proposed that some studied stellar groups are also associated with disrupted stellar clusters. In general the identification of a stellar moving group formed by this mechanism might not be an easy task, because the perturbed cluster stars could follow orbits quite distinct from the original cluster orbit, i.e. the ‘tube’ could be very wide, thus the expected clumping in the U–V plane would not be clear. The detailed chemical analysis required in the identification of a disruption origin restricts the connection of a moving group and a possible parent cluster; e.g., the results of [Wylie-de Boer et al. \(2010\)](#); [Navarrete et al. \(2015\)](#) respect to the possible association of the Kapteyn group with the globular cluster ω Centauri. Considering a disruption on a larger scale, a possible origin of

moving groups in the Galactic halo has been associated to the relics of satellite galaxies disrupted by our own Galaxy (Helmi et al. 1999; Meza et al. 2005; Zhao et al. 2014).

Other proposed mechanisms for the origin of moving groups have been considered in the literature. The effect of the spiral arms and the Galactic bar has been studied by Antoja et al. (2009a,b, 2010, 2011); Quillen & Minchev (2005) using test-particle simulations to compare with the observed distribution of disk stars in the U–V plane in the solar neighborhood. For old moving groups in eccentric orbits, trapping of stars by resonances due to spiral arms or a bar has been proposed by Dehnen (1998). A recent alternative mechanism has been analyzed by Olano (2016, 2015), proposing that some moving groups in the solar neighborhood were born by the desintegration of an old gaseous supercloud or by the capture of stars due to a local giant interstellar cloud.

The present analysis is concerned in particular with the two moving groups G18-39 and G21-22 in the Galactic halo, which were identified by Silva et al. (2012). In that study the suggested origin of these groups was related with the disruption of the globular cluster ω Centauri, as inferred by theoretical simulations made by Meza et al. (2005). Here we consider an alternative explanation for the presence of these two groups in the solar neighborhood, which is directly connected with resonant trapping of 3D orbits by resonances on the Galactic plane generated by the Galactic bar. We have analyzed this trapping mechanism in a previous study (Moreno et al. 2015). In Section 2 we list the updated data for the stars in both groups G18-39 and G21-22. The employed non-axisymmetric Galactic potential is presented in Section 3, and the resonant trapping of stars in both groups is analyzed in some detail in Section 4. The comparison between the observed and resulting resonant U–V velocity distributions is given in Section 5, and our conclusions are summarized in Section 6.

2. DATA FOR THE TWO MOVING GROUPS

The kinematic parameters of the stars in the two groups G18-39 and G21-22 are listed in Silva et al. (2012). Some of these parameters have been updated using recent published data. The radial velocities have been selected from the literature using always the most precise and accurate values available, generally with errors less than $\pm 1.0 \text{ km s}^{-1}$, such as those of Latham et al. (2002), Abolfathi et al. (2017), Nissen & Schuster (2010), and Pourbaix et al. (2004). Gontcharov (2006) has given radial velocities with errors over a range ± 0.2 to $\pm 4.8 \text{ km s}^{-1}$, and for the more southern stars the RAVE survey (Kunder et al. 2017; Siebert et al. 2011; Zwitter et al. 2008) errors over ± 1.0 to $\pm 2.8 \text{ km s}^{-1}$. Nine stars, which were included in the catalogue employed in our previous publication related with moving groups (Moreno et al. 2015), still retain their older radial velocities with errors from $\approx \pm 5$ to $\approx \pm 7 \text{ km s}^{-1}$. The median error of the radial velocities used here is $\pm 0.28 \text{ km s}^{-1}$.

Table 1 lists the parameters employed in our computations. The star identification is that given in Silva et al. (2012). A convenient reference number is listed in the second column, and in the following columns appear the positions, radial velocity, proper motions, uncertainties in the radial velocity and proper motions, and distance from the Sun with uncertainty.

Table 1. Data for the two moving groups

ID	Number	α (degrees)	δ (degrees)	V_{rad} (km sec^{-1})	μ_{α} (mas yr^{-1})	μ_{δ} (mas yr^{-1})	σV_{rad} (km sec^{-1})	$\sigma \mu_{\alpha}$ (mas yr^{-1})	$\sigma \mu_{\delta}$ (mas yr^{-1})	D (pc)	σD (pc)
GROUP G18-39											
G31-26	1	2.0818292	−5.2485278	−217.05	353.000000	−123.000000	0.3	5.000000	5.000000	200.3	20.0
HD3567	2	9.6332007	−8.3115530	−48.20	20.664299	−546.521926	0.2	0.089203	0.062938	115.3	4.0
G70-33	3	15.9760000	−3.8539444	−83.42	342.000000	−69.000000	0.3	5.000000	5.000000	246.3	24.6
G34-45	4	25.7032083	22.6173056	−277.68	87.380000	−304.720000	0.2	10.000000	10.000000	133.7	16.6
LP709-053	5	33.0099844	−14.0082561	−7.00	263.849965	−62.525949	7.0	2.173218	1.119031	263.9	26.1
G36-47	6	44.3338936	26.2805580	88.93	260.765338	−226.759889	0.2	1.606972	0.747114	224.5	24.8
G86-39	7	80.7978333	33.1841944	214.30	412.865000	−720.029000	0.3	10.000000	10.000000	81.1	8.1
G98-53	8	93.4577354	33.4158976	144.49	22.658701	−325.715595	0.2	5.754996	6.037369	177.7	7.1
−48 : 2445	9	100.3614907	−48.2198975	319.60	64.566503	217.261808	7.0	1.083189	0.596698	186.2	9.6
G87-13	10	103.7345667	35.5162722	206.53	53.500000	−241.700000	0.2	3.900000	3.800000	256.3	25.6
G89-014	11	110.6316879	8.8191592	−36.02	151.047078	−269.304977	1.2	0.157074	0.082924	220.5	12.0

Table 1 continued on next page

Table 1 (*continued*)

ID	Number	α (degrees)	δ (degrees)	V_{rad} (km sec ⁻¹)	μ_{α} (mas yr ⁻¹)	μ_{δ} (mas yr ⁻¹)	σV_{rad} (km sec ⁻¹)	$\sigma \mu_{\alpha}$ (mas yr ⁻¹)	$\sigma \mu_{\delta}$ (mas yr ⁻¹)	D (pc)	σD (pc)
LP490-061	12	160.9967490	12.8011075	213.00	-149.289457	-97.293485	7.0	2.422196	1.275121	418.9	129.3
G120-15	13	166.5854875	31.2140639	131.53	-202.680000	-126.650000	0.2	10.000000	10.000000	318.0	31.8
G10-03	14	167.5109792	-2.7905361	202.20	141.000000	-468.000000	0.8	5.000000	5.000000	111.9	13.9
-24 : 9840	15	174.0112167	-24.8728417	164.05	-21.200000	-215.700000	1.0	3.100000	2.900000	309.3	30.9
HD101063	16	174.4168530	-28.8514150	183.40	-313.626643	-15.760882	0.3	0.076786	0.051859	249.6	17.5
G176-53	17	176.6464773	50.8818562	64.40	-870.070000	-543.760000	0.2	1.080000	0.890000	76.0	7.6
G66-30	18	222.5325179	0.8408762	-115.08	-283.780000	-104.710000	0.1	2.870000	2.470000	233.1	23.3
G15-24	19	232.6723763	8.3940935	-88.51	-391.277812	-116.995738	0.2	0.340198	0.191280	159.3	6.8
LP636-003	20	311.2551750	-1.6820528	-57.00	-38.300000	-186.100000	7.0	5.500000	5.500000	339.8	33.9
G187-30	21	317.8235693	33.5249133	-340.60	502.936813	159.151139	0.6	0.189435	0.313993	99.4	2.7
-03 : 5166	22	319.3293250	-2.7486250	-122.00	-103.400000	-248.000000	7.0	2.500000	2.300000	260.4	26.0
G18-39	23	334.6533014	8.4453971	-234.77	283.316895	-102.184230	0.2	0.212514	0.149986	154.6	5.8
LP877-025	24	343.3748958	-23.9131306	117.78	-24.700000	-400.500000	9.5	2.300000	2.100000	195.4	19.5
G157-85	25	354.1300417	-8.4312222	-82.0	254.000000	-144.000000	7.0	5.000000	5.000000	258.7	25.9
GROUP G21-22											
G02-38	1	21.7298294	12.0056807	-171.16	-10.988957	-359.179492	0.3	3.316039	0.712774	185.6	17.2
G82-42	2	70.5000208	-4.2794694	-8.62	2.500000	-347.600000	0.3	4.600000	4.200000	218.2	21.8
G108-48	3	105.4036445	6.4080035	-87.77	3.130000	-674.110000	0.3	3.200000	2.390000	133.4	13.3
HIP36878	4	113.7224627	-10.3881404	89.00	424.679519	-482.042040	4.8	0.135706	0.118253	106.2	2.8
G116-45	5	146.1589536	38.6096750	-33.89	210.121664	-238.618536	0.2	1.179395	1.077341	303.3	74.3
G161-73	6	146.4082615	-4.6756279	120.92	150.156734	-251.937567	0.2	2.187828	1.692420	279.1	48.4
G146-56	7	159.9603750	42.1514444	-104.40	81.710000	-212.860000	0.3	10.000000	10.000000	310.0	31.0
G119-64	8	168.2003636	35.7267285	-196.25	71.001036	-510.780372	0.2	0.122860	0.092605	139.5	4.5
G139-16	9	257.4474167	8.0737500	40.77	-100.000000	-410.000000	0.2	14.000000	7.000000	197.2	19.7
LP808-022	10	267.6524583	-16.9841111	200.00	-60.000000	-216.000000	7.0	5.000000	5.000000	315.4	31.5
G154-25	11	267.6541667	-16.9866667	200.00	-60.500000	-216.400000	7.0	5.500000	5.500000	313.3	31.3
G21-22	12	279.7904792	0.1206528	59.45	-168.900000	-446.200000	0.2	1.500000	1.500000	158.9	15.9

3. THE GALACTIC MODEL

The Galactic orbits of the stars in both groups G18-39 and G21-22 were computed in a Galactic potential including axisymmetric and non-axisymmetric components. The base for this potential is the axisymmetric model of [Allen & Santillan \(1991\)](#). All the mass in the spherical bulge component in this model has been employed to construct a Galactic prolate bar with a similar distribution of mass (i.e., the surfaces of equal density are concentric spheroids with the same eccentricity), whose potential is given in [Pichardo et al. \(2004\)](#) and has a density law and geometry which approximates a model of [Freudenreich \(1998\)](#) of *COBE*/DIRBE observations of the Galactic center. After this transformation, the whole potential, including the axisymmetric components, was rescaled to the Sun's galactocentric distance $R_0 = 8.3$ kpc and LSR (Local Standard of Rest) velocity $\Theta_0 = 239$ km s⁻¹ ([Brunthaler et al. 2011](#)). The employed prolate bar, with a mass of $1.6 \times 10^{10} M_{\odot}$, is an approximation for the more detailed model of the inner Galactic region given by [Portail et al. \(2017\)](#), which consists of a boxy/peanut bulge aligned with a long bar, both components giving a total mass around $1.88 \times 10^{10} M_{\odot}$.

The present orientation of the major axis of the Galactic bar and its angular rotation speed was revised in our earlier study of resonant trapping in the Galactic halo ([Moreno et al. 2015](#)). There the values 20° and 55 km s⁻¹ kpc⁻¹ were considered for these two parameters. Here we extend their possible range of values inferred by recent analysis of bar parameters based on the study of the Hercules stream ([Hunt et al. 2018](#); [Pérez-Villegas et al. 2017](#)), and the model of [Portail et al. \(2017\)](#) mentioned above, which propose values of the orientation angle up to around 30° and angular speeds down to around 40 km s⁻¹ kpc⁻¹. We include these extensions in our computations. Table 2 summarizes the values of the parameters in the employed non-axisymmetric Galactic model, including the used Solar motion ([Schönrich](#)

et al. 2010), with U negative towards the Galactic center.

Table 2. Parameters Employed in the Non-Axisymmetric Galactic Potential

Position and Velocity of the LSR and Solar Velocity	
R_0	$8.3 \pm 0.23 \text{ kpc}$ ^(a)
Θ_0	$239 \pm 7.0 \text{ km s}^{-1}$ ^(a)
$(U, V, W)_\odot$	$(-11.10, 12.24, 7.25) \pm (1.20, 2.10, 0.60) \text{ km s}^{-1}$ ^{(a),(b)}
Properties of the Galactic Prolate Bar	
Law Density	$\rho(a) \propto \text{sech}^2(a)$ ^{(c),(d)} ; a =major semiaxis of prolate similar surfaces
Mass (scaled Bulge Mass in Allen & Santillan (1991) Galactic Model)	$1.6 \times 10^{10} M_\odot$ ^(e)
Present position of major axis	$20^\circ, 25^\circ, 30^\circ$ ^(f)
Angular velocity Ω_b	$40, 45, 50, 55, 60 \text{ km s}^{-1} \text{ kpc}^{-1}$ ^{(f),(g),(h)}

^(a)Brunthaler et al. (2011)

^(b)Schönrich et al. (2010)

^(c)Freudenreich (1998)

^(d)Pichardo et al. (2004)

^(e)Allen & Santillan (1991)

^(f)Hunt et al. (2018)

^(g)Pérez-Villegas et al. (2017)

^(h)Portail et al. (2017)

4. RESONANT TRAPPING OF THE TWO MOVING GROUPS

In this section we consider the first part of our analysis of the two groups G18-39 and G21-22, focussing in the possible trapping of the stars in these groups by resonances on the Galactic plane generated by the Galactic bar, which may help to understand their identification as star groups.

4.1. The Characteristic Energy- J plane

In our earlier study of resonant trapping in the Galactic halo (Moreno et al. 2015, hereafter Paper I), the orbits of 1642 halo and disk stars in the solar neighborhood were computed in the non-inertial reference frame where the bar component of the potential is at rest. In that study we employed the boxy bar given in Pichardo et al. (2004). Every orbit was computed backward in time during 10 Gyr and a characteristic energy- J diagram was found to be useful in the orbital analysis. J is the orbital Jacobi constant per unit mass, and the characteristic energy was defined as $(E_{\min} + E_{\max})/2$, with E_{\min} , E_{\max} the minimum and maximum values of the non-constant orbital energy per unit mass with respect to the *inertial* Galactic frame. In this diagram, which employes in general 3D orbits, some accumulations of points appear in certain regions, which were found to be related with corresponding positions in this diagram of families of periodic orbits on the Galactic plane, i.e., 2D orbits, generated by the bar. Thus, in these regions, 3D orbits may be trapped by resonant 2D orbits on the Galactic plane.

In the present study the orbits of the stars in both groups were also computed backward in time during 10 Gyr for each value of the angular rotation speed of the Galactic bar, Ω_b , listed in Table 2, and with their kinematic results characteristic energy- J diagrams were plotted in each case. To have a background of comparison, the orbits of the 1642 stars employed in Paper I were again represented in these diagrams (in fact, the members of the two groups G18-39 and G21-22 are included in the 1642 stars sample). The results given in this and the following sections correspond to an initial orientation of 20° for the major axis of the Galactic bar; the values 25° and 30° gave similar orbits in both groups.

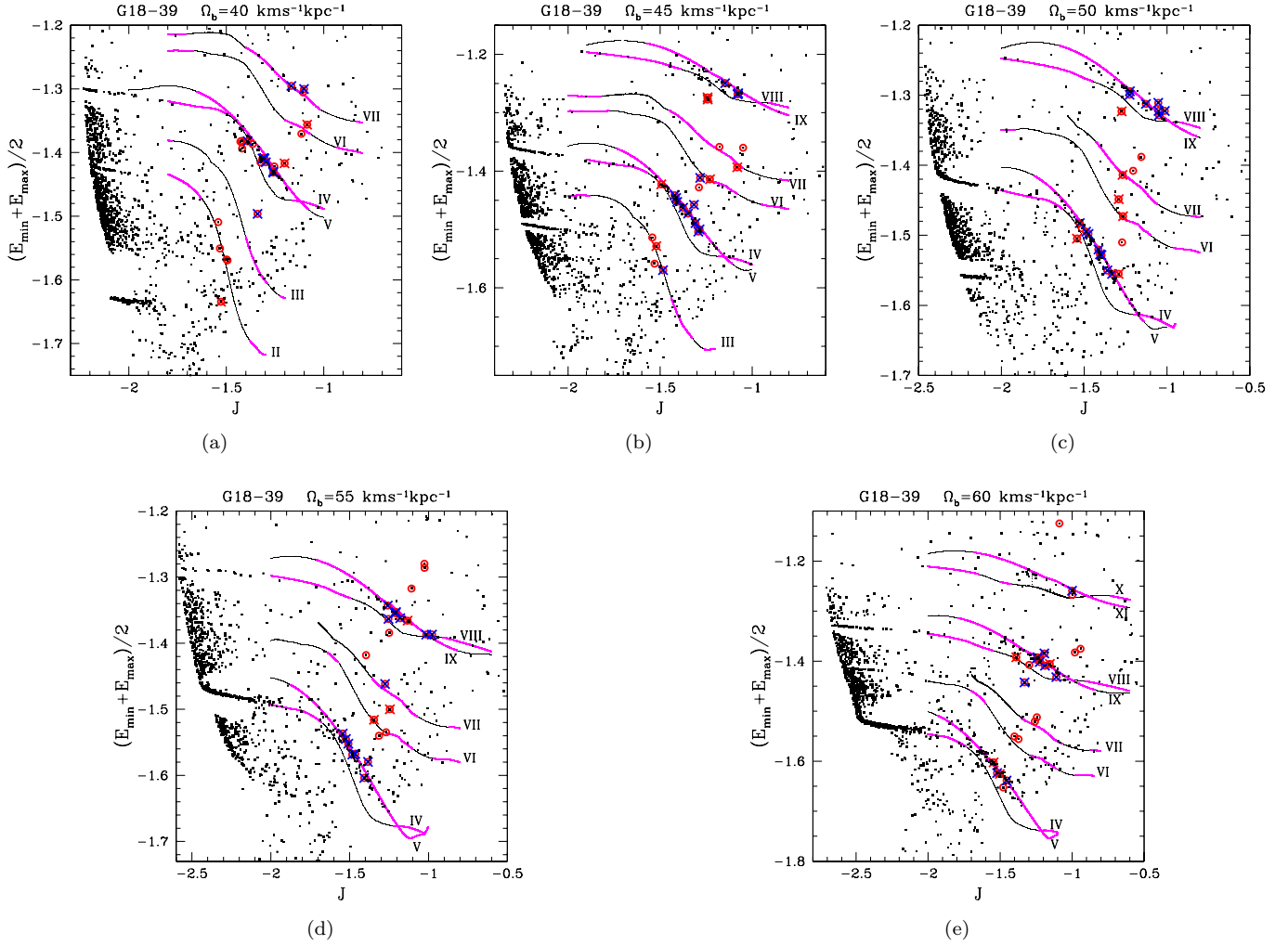


Figure 1. Characteristic energy– J diagram for the group G18-39 using $\Omega_b=40,45,50,55,60 \text{ km s}^{-1} \text{ kpc}^{-1}$. The units in $(E_{\min} + E_{\max})/2$ and J are $10^5 \text{ km}^2 \text{ s}^{-2}$. The small black points correspond to the 1642 stars sample. The curves are some of the main 2D resonant families generated by the Galactic bar. The magenta and black parts of each curve are stable and unstable points along the family, respectively. Each curve is numbered as in Paper I. The red-circled points belong to the group. Of these points, those with a blue cross represent orbits trapped by resonances during a time interval greater than 5 Gyr, the points with a red cross are orbits trapped during less than 5 Gyr; points without a cross represent orbits not trapped by resonances. See main text.

In Figures 1 and 2 we show the characteristic energy– J diagrams, which include the results obtained for the two groups under different values of the rotation speed Ω_b . The units employed for $(E_{\min} + E_{\max})/2$ and J are $10^5 \text{ km}^2 \text{ s}^{-2}$. The small black points are part of the 1642 stars sample. In these diagrams it is useful to show the loci of points or curves corresponding to some of the main 2D resonant families generated by the Galactic bar, as well as the stable and unstable parts of each curve. Some of these curves are shown in Figures 1 and 2. As in Paper I, the curves were computed using Poincaré diagrams combined with a Newton-Raphson scheme, and the type of stability computed with the method given by Hénon (1965); see also Contopoulos (2002). The curves are numbered with notation in Paper I. The magenta and black parts of each curve correspond respectively to stable and unstable points along the family. Only parts of these curves are shown; they can be extended to the left and right in all figures. The red-circled points in these figures, some of which have a blue or red cross, correspond in each case to one of the two analyzed groups, and are commented in the following subsections. Some important features can be noticed in the characteristic energy– J diagrams shown in Figures 1 and 2: (a) for each value of Ω_b the points of both groups, and all the background points, distribute in different ways, (b) the resonant family curves move downwards as Ω_b is increased and new families appear at the top, (c) the majority of points in a given group tend to accumulate around some resonant families.

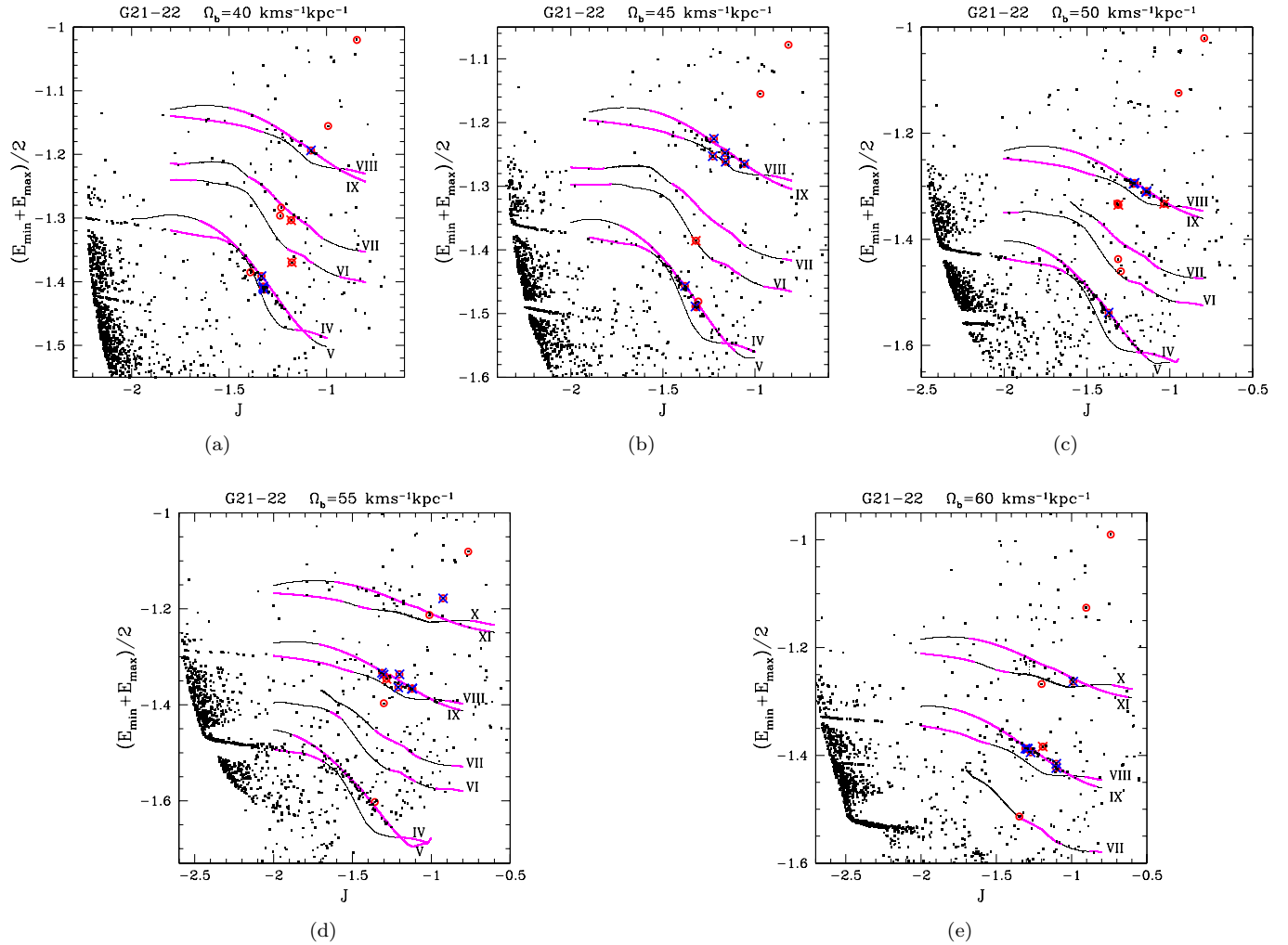


Figure 2. As in Figure 1, here the corresponding diagrams for the group G21-22.

4.2. The two Moving Groups in the Characteristic Energy– J plane

To represent the points of a given group in the characteristic energy– J diagrams, the corresponding orbits were analyzed to see if they were trapped or not by resonances. A first indication is obtained with a visual inspection of the orbits. During the total computed time of 10 Gyr each 3D star orbit in a group was plotted projected on the Galactic plane, as viewed in the *non-inertial* reference frame where the bar is at rest. This projection was compared during several subintervals of time with different orbital forms of 2D resonant families due to the bar, which are already given in figures presented in Paper I. As in general the projection will not coincide with the closed curve of a 2D resonant orbit, the visual criterion to establish when a 3D orbit was trapped by a given resonant family consisted in the comparison of the projected orbit with expected associated tube orbits on the Galactic plane around *stable* points of this family.

Figure 3 shows an example of an orbit trapped by a resonance according to a visual inspection. The 3D orbit corresponds to star number 11 in Table 1 for the group G18-39. The value of Ω_b is $50 \text{ km s}^{-1} \text{ kpc}^{-1}$. Frame (a) shows the meridional orbit, and frame (b) shows the orbit projected on the Galactic plane as viewed in the non-inertial reference frame of the bar. The x' -axis points along the major axis of the bar. The orbit is clearly trapped by a resonance on the Galactic plane. The trapping family is the one numbered as V in the corresponding characteristic energy– J diagram shown in frame (c) of Figure 1, as can be inferred by the comparison of the projected orbit with the forms of resonant 2D orbits in this family given in Paper I (see figure 14 in that paper). For the same value of the Jacobi constant J in the 3D orbit, frame (c) in Figure 3 shows the corresponding 2D *stable* resonant orbit in family V, and frame (d) shows a tube orbit on the Galactic plane around this resonant orbit which resembles the projected

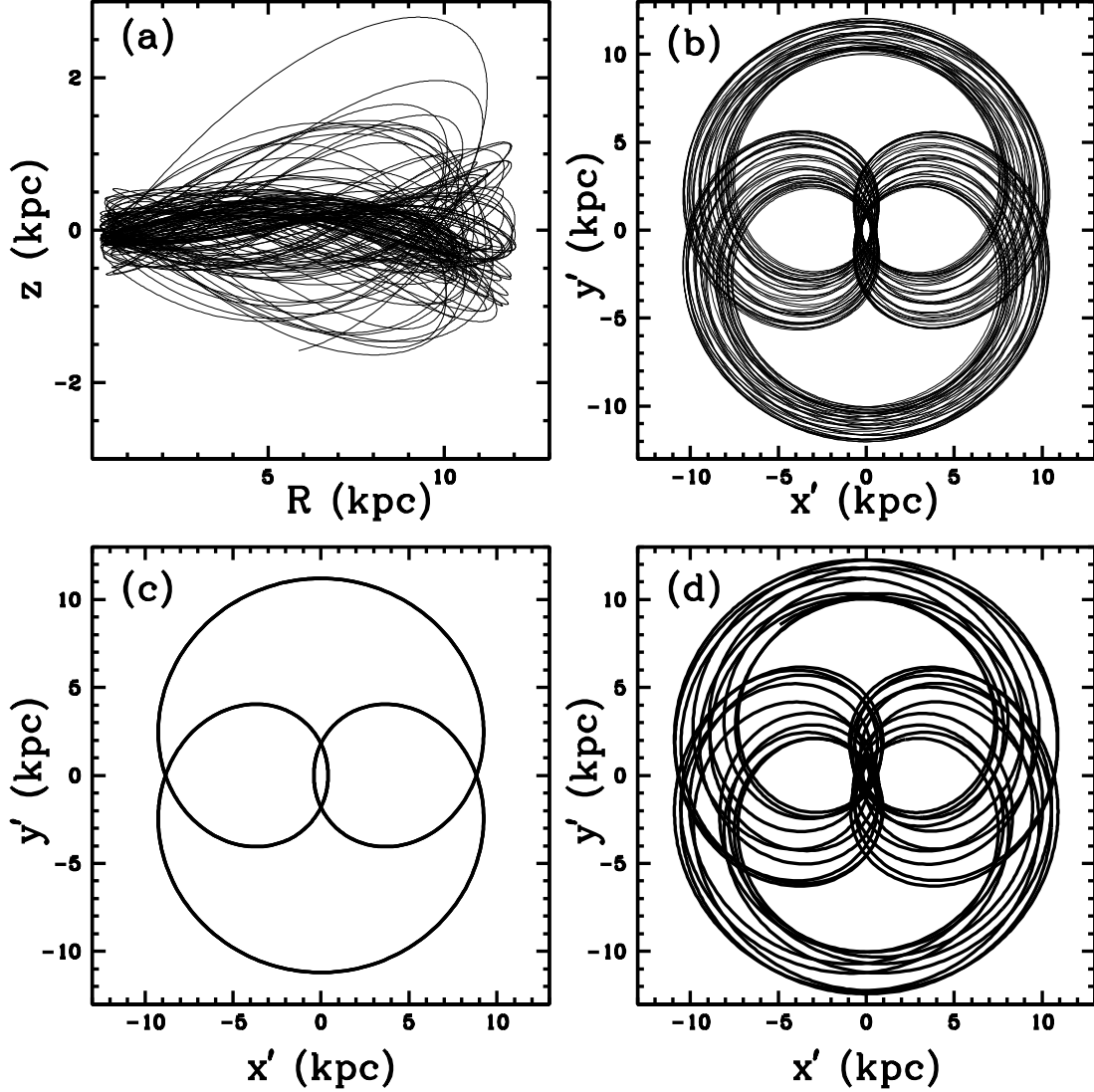


Figure 3. An example of a trapped orbit; for star number 11 in the group G18-39, with $\Omega_b = 50 \text{ km s}^{-1} \text{ kpc}^{-1}$. The meridional orbit is shown in frame (a) and the projected orbit on the Galactic plane x', y' (with the x' -axis pointing along the major axis of the bar) in the non-inertial reference frame of the bar is shown in (b). This projected orbit is associated with the resonant family V; see figure 14 in Paper I. Frame (c) shows the *stable* resonant orbit in family V with the same value of the Jacobi constant J as in the 3D orbit of the star. Frame (d) shows a tube orbit on the Galactic plane around this resonant orbit. A visual comparison of frames (b) and (d) shows that the 3D orbit is trapped by family V.

orbit in frame (b). Thus, we conclude that the orbit is trapped by family V.

We considered a second, complementary and more quantitative, criterion to see if an orbit is trapped or not by resonances. As was done in the case shown in Figure 3, for the resulting value of J in the 3D orbit of a star in a group the corresponding 2D *stable* resonant orbit of the inferred trapping family was localized. A series of tube orbits on the Galactic plane were computed around this resonant orbit and were represented in a Poincaré diagram. In particular, to construct this diagram we localized the points where the orbits cross the y' -axis. This diagram corresponds to 2D orbits on the Galactic plane; thus, the 3D orbit of the star is not directly represented in this diagram. We chose the natural extension of localizing the points where the 3D orbit crosses the $x' = 0$ plane (at different z' positions with respect to the Galactic plane), and with the corresponding values of the position y' and velocity $v_{y'}$, this orbit was plotted in the Poincaré diagram. In this diagram the points of the 3D orbit will not necessarily lie on a given invariant curve, as the 2D tube orbits do, but we expect that if the 3D orbit is trapped, its points will distribute among the curves representing the tube orbits.

To illustrate this last procedure, Figures 4 and 5 show some Poincaré diagrams associated to orbits of some stars in groups G18-39 and G21-22 which by the visual criterion, and by the results presented in these diagrams, have been considered as trapped by resonant orbits on the Galactic plane. In Figure 4 nine examples are shown for the group G18-39 with $\Omega_b = 50 \text{ km s}^{-1} \text{ kpc}^{-1}$, and Figure 5 shows six examples for the group G21-22 with $\Omega_b = 55 \text{ km s}^{-1} \text{ kpc}^{-1}$. The number in each frame is the number of star in the group; see Table 1. The trapping family in Figure 4 is family V, and in Figure 5 is family IX. The orbital form of periodic orbits in these families can be seen in figures 14 and 18 in Paper I; Figure 6 gives an example of a periodic orbit in this family IX. The black points in each frame of Figures 4 and 5 correspond to some tube orbits around the stable periodic orbit. The red points correspond to the 3D orbit in the group, which approximately distribute among the curves of the tube orbits. In particular, the frame with number 11 in Figure 4 gives the result for the star in Figure 3. The three examples in Figures 4 and 5 in which some points appear with a magenta color indicate cases where the orbit is trapped only during some interval of time, less than the 10 Gyr considered in the orbit; the magenta points correspond to that limited interval. For all considered values of Ω_b we found that some of the 3D orbits could be trapped only in some intervals of time, as in their projection on the plane x', y' they were oscillating inside and outside a tube orbits region. Thus, if the projected orbit was approximately inside the tube region in a certain interval of time, this time was considered as a contribution for the total trapping time of the corresponding resonant trapping family. In the majority of cases the total trapping time was equal to the total computed orbital time of 10 Gyr. In Section 5.2 some more detail is given on the behavior of an orbit trapped during some limited interval of time, and non-trapped orbits.

Returning to Figures 1 and 2, of the red-circled points belonging to a group, those with a blue or red cross represent stars with orbits trapped by resonances during a time interval greater, or less than 5 Gyr, respectively. Group points without a cross represent orbits not trapped by resonances. The division at 5 Gyr is arbitrary, just to show long and short trapping. Some points to notice from these figures are:

1. Resonant trapping may occur in or near the stable parts of a resonant family.
2. There are group points which may be very close to a *stable* part of a resonant family but are *not* trapped. In a given Galactic potential, general conditions for a 3D orbit to be trapped by a 2D resonance on the Galactic plane remain to be analyzed. In Section 5.2 some comments on non-trapped orbits are given.
3. Resonant trapping of a given star in a group depends on the value of Ω_b . As noted above, the distribution of points in a characteristic energy–J diagram varies strongly with the value of this parameter.

In Table 3 we give a summary of the results shown in Figures 1 and 2. For each star in a group, numbered as in Table 1, and for each value of Ω_b , the trapping family and the trapping time in units of Gyr are given in each entry. Empty spaces correspond to non-trapped orbits. Where “other” appears for the trapping family, it means that there are few missed resonant families which were not computed in this study and in Paper I; they are not very relevant in the results. The trapping families III \perp and VI \perp denote the resonant families perpendicular to families III and VI given in Paper I (its figures 12 and 15), i.e., those families rotated 90°. Examples of perpendicular families already appeared in Paper I: IV and V, VIII and IX, X and XI. In regions where the points of groups G18-39 and G21-22 distribute, families IV, VIII, and X have unstable parts but families V, IX, and XI have stable parts, thus in these regions the later are the possible trapping families. Related to this, the trapped points with a blue cross in frame (b) of Figure 1 which lie close to *unstable* parts of curves III and VI (these points correspond to stars 19 and 17 in group G18-39) are actually trapped by near *stable* parts of families III \perp and VI \perp (not shown in the figures).

Our main conclusions with the results in Figures 1 and 2 are:

1. The majority of stars in both groups G18-39 and G21-22 are trapped by 2D resonances on the Galactic plane generated by the Galactic bar.
2. There is not a single trapping family in each group; the main trapping families in both groups are the families V and IX, with family IX dominating in G21-22. Thus, it appears that the majority of stars in both groups are members of the supergroups of stars in the Galaxy trapped by the resonant families V and IX.
3. In the group G18-39 the interval 45–55 $\text{km s}^{-1} \text{ kpc}^{-1}$ in Ω_b produces the major number of trapped orbits by families V and IX, and in the group G21-22 the corresponding interval is 45–60 $\text{km s}^{-1} \text{ kpc}^{-1}$.
4. For a given star in a group, a possible resonant trapping depends strongly on the value of Ω_b .

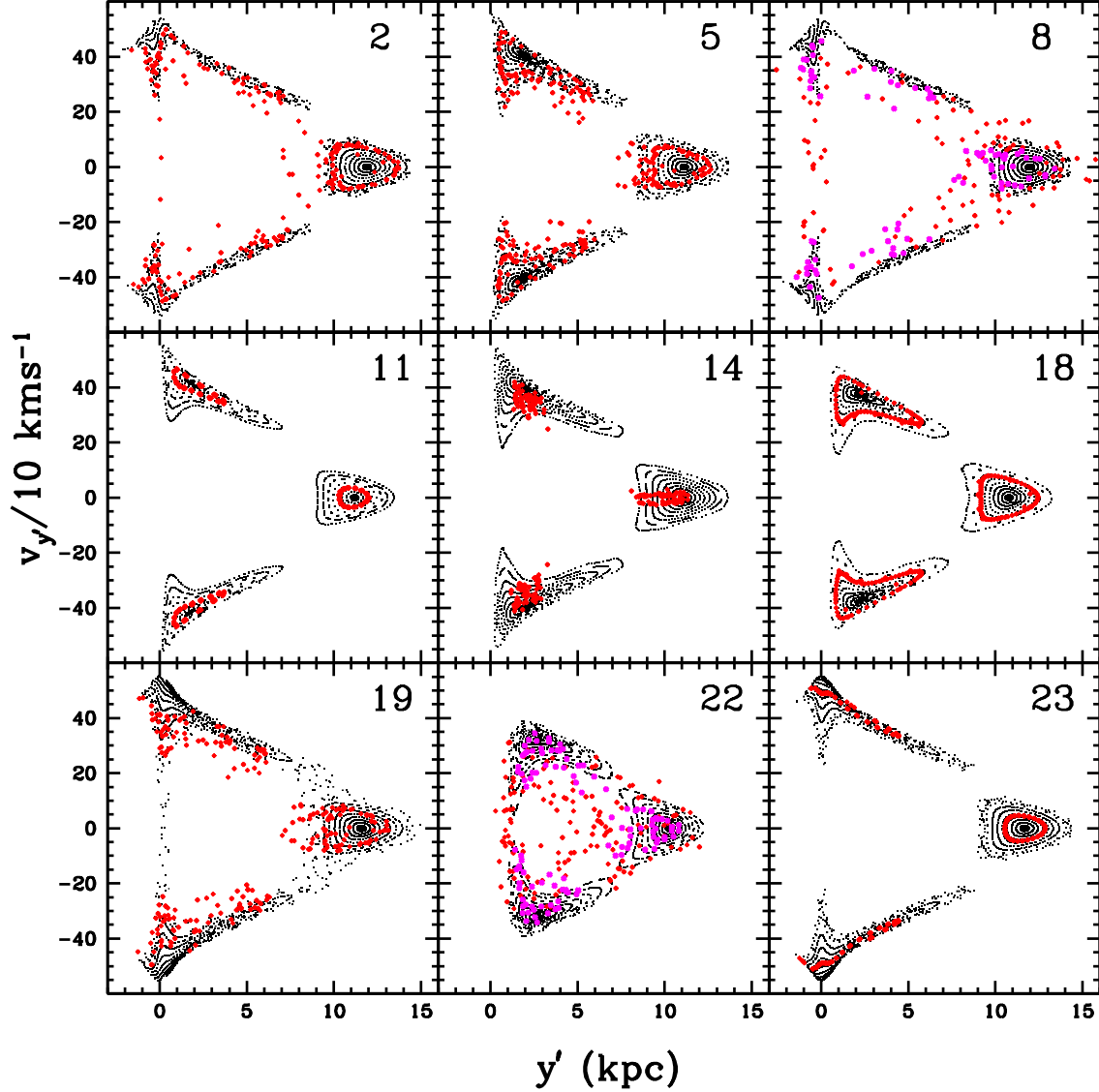


Figure 4. Examples of extended Poincaré diagrams for stars in the group G18-39 with $\Omega_b = 50 \text{ km s}^{-1} \text{ kpc}^{-1}$. The number in each frame is the number of star in the group. The black points show some tube orbits around the stable periodic orbit in the trapping family (family V in this figure), with the same value of J as the 3D orbit in the group. The red points correspond to the 3D orbit in the group. The two frames with points in magenta color are cases in which the orbit is approximately trapped during a time interval less than 10 Gyr, shown by these magenta points.

Table 3. Trapping family and trapping time during 10 Gyr

Number	$\Omega_b \text{ (km s}^{-1} \text{ kpc}^{-1}\text{)}$				
	40	45	50	55	60
GROUP G18-39					

Table 3 continued on next page

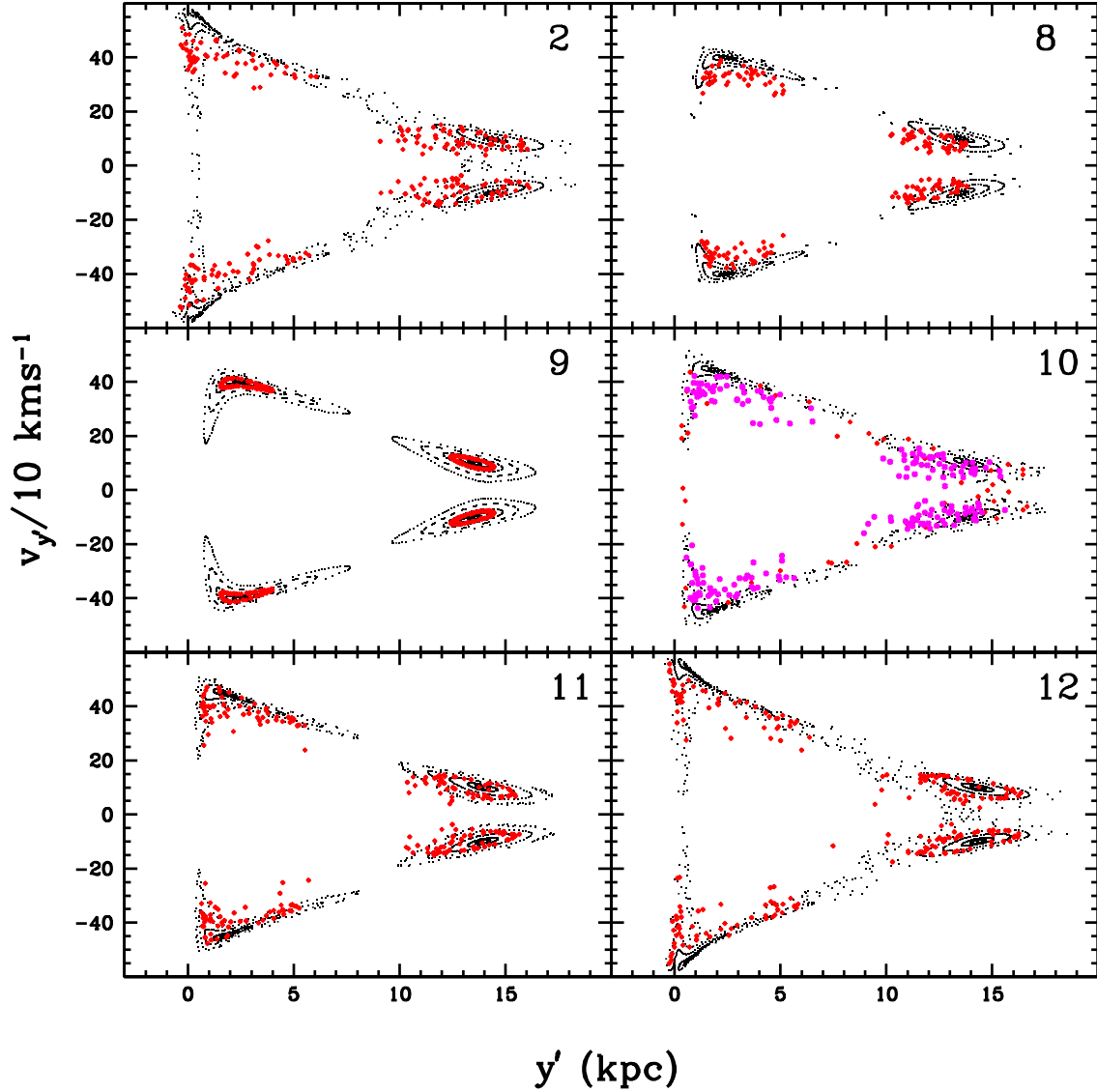


Figure 5. As in Figure 4, here for the group G21-22 with $\Omega_b = 55 \text{ km s}^{-1} \text{ kpc}^{-1}$. The trapping family in this figure is family IX.

Table 3 (continued)

Number	$\Omega_b \text{ (km s}^{-1} \text{ kpc}^{-1}\text{)}$				
	40	45	50	55	60
1	VII;4	—	IX;5.5	IX;10	—
2	—	—	V;10	V;10	V;10
3	—	IX;10	IX;8	—	—
4	—	V;10	V;10	—	—
5	—	V;10	V;10	—	IX;2.5
6	—	~VI;4	—	IX;8.5	IX;4.5
7	V;10	IX;4	IX;10	IX;10	IX;10
8	—	—	V;4.5	V;10	V;4
9	V;10	—	X;4	IX;10	IX;10

Table 3 continued on next page

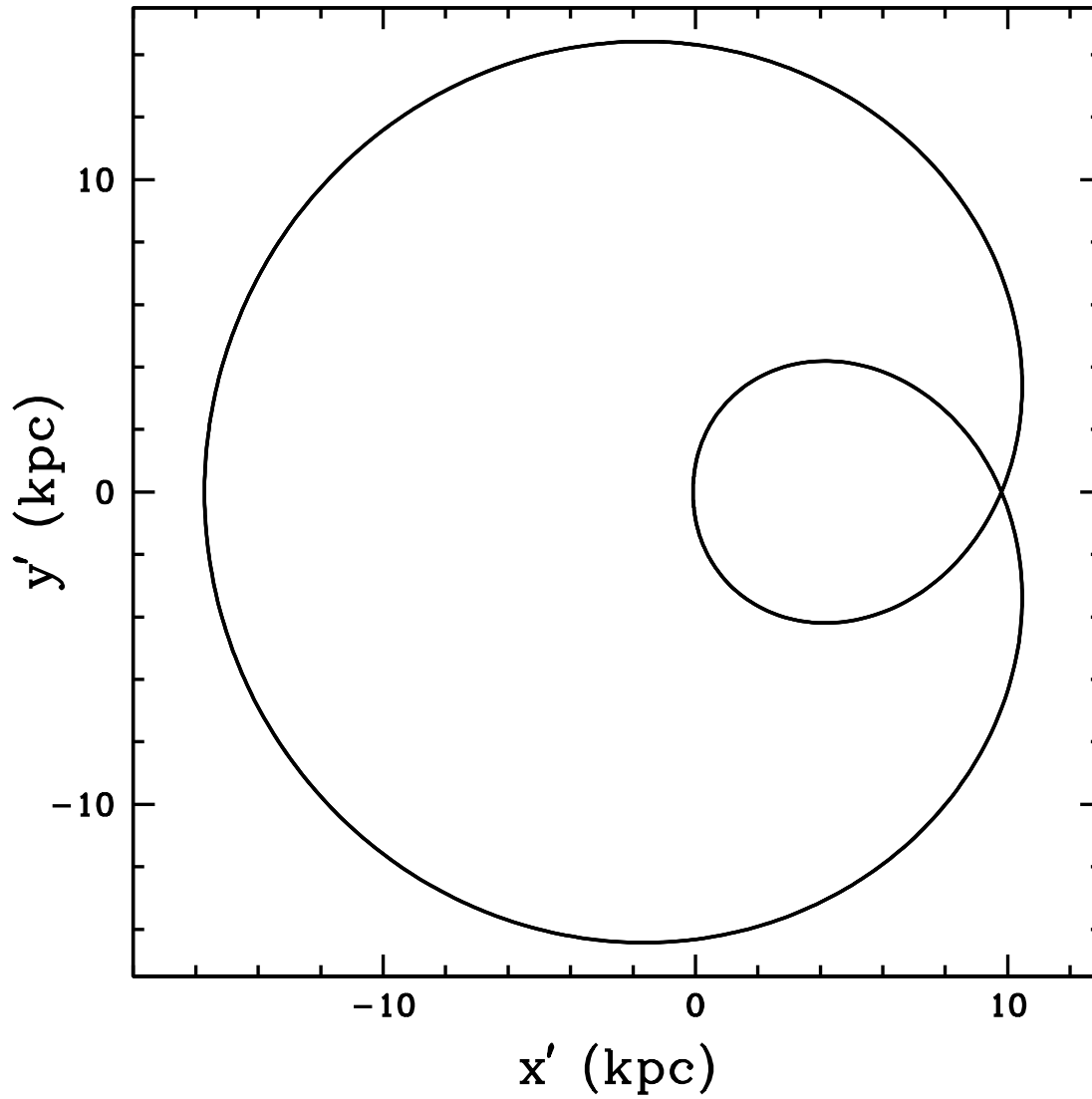


Figure 6. An example of a periodic orbit in family IX.

Table 3 (*continued*)

Number	Ω_b (km s ⁻¹ kpc ⁻¹)				
	40	45	50	55	60
10	V;10	V;10	VI \perp ;3.5	VI \perp ;4	IX;10
11	—	V;10	V;10	V;10	—
12	—	other;4	IX;10	IX;10	—
13	V;10	IX;3.5	IX;5	IX;10	IX;8
14	—	V;10	V;10	V;7	—
15	—	V;6	VI;3	other;10	—
16	VII;10	IX;10	IX;10	—	—
17	V;10	VI \perp ;6	other;4.5	IX;5	IX;10
18	—	V;10	V;10	VI \perp ;2	IX;6

Table 3 continued on next page

Table 3 (*continued*)

Number	Ω_b (km s ⁻¹ kpc ⁻¹)				
	40	45	50	55	60
19	—	III \perp ;5	V;10	V;10	V;5
20	other;2.5	III \perp ;2	—	V;10	V;4
21	VII;5	IX;8	IX;5	—	XI;10
22	other;10	V;5	V;4	—	—
23	—	other;4	V;10	V;10	—
24	V;4	—	—	IX;4	IX;8
25	V;10	V;8	—	—	IX;4.5
GROUP G21-22					
1	V;10	—	—	IX;5	IX;10
2	V;10	VI;3	—	IX;10	IX;8
3	—	—	—	~XI;9.5	—
4	—	V;10	V;10	—	—
5	—	—	—	—	—
6	IX;6	IX;10	IX;2.5	—	XI;5
7	V;10	V;8	~VI \perp ;3	—	IX;10
8	VI;4	IX;8	IX;10	IX;10	IX;5
9	VI;4	IX;6	IX;6	IX;10	IX;10
10	—	IX;8	IX;10	IX;8	IX;3.5
11	—	IX;8	IX;10	IX;10	—
12	V;10	—	IX;2.5	IX;10	IX;10

4.3. Orbits

In this part we present some examples of star orbits in the two groups G18-39 and G21-22. Figure 7 shows the orbits of 24 of the 25 stars in the group G18-39, with $\Omega_b = 50$ km s⁻¹ kpc⁻¹. The meridional orbits are shown in frames (a) and (b), and the corresponding projected orbits on the Galactic plane in the non-inertial reference frame of the bar, are shown in frames (c) and (d). The star number is given inside each small frame. The twelve stars in frames (a),(c) and the first three in frames (b),(d) have orbits trapped in an interval of time greater or equal to 5 Gyr. See the corresponding column in Table 3 for the trapping family and trapping time. Notice the different maximum z-distances reached in each orbit. The six orbits in red color in frames (b),(d) are approximately trapped in an interval of time less than 5 Gyr, and the last three in these frames are non-trapped orbits. For the group G21-22, Figure 8 gives the meridional (frame (a)) and projected (frame (b)) orbits of the 12 stars in this group, with $\Omega_b = 55$ km s⁻¹ kpc⁻¹. The first eight stars have trapped orbits in an interval of time greater or equal to 5 Gyr. The last four stars have non-trapped orbits. In this group and with the given value of Ω_b , the main trapping family is family IX.

4.4. Monte Carlo simulations

To see the effect of the uncertainties in the kinematic parameters of the stars in both groups G18-39 and G21-22, listed in Table 1, two representative Monte Carlo simulations are given in this subsection. For each star, 500 orbits were computed with initial conditions drawn from the set of varying kinematic parameters, including the Solar motion, with R_0 , Θ_0 of the LSR and Ω_b of the bar kept fixed. Figure 9 shows in frame (a) the results with $\Omega_b = 50$ km s⁻¹ kpc⁻¹ in the group G18-39, and in frame (b) the results with $\Omega_b = 55$ km s⁻¹ kpc⁻¹ in the group G21-22. The red points are the resulting average positions and the blue lines their associated dispersions. Comparing with the results obtained in frame (c) of Figure 1 and frame (d) of Figure 2 using the mean values of the parameters, approximate accumulations around resonant families V and IX are recovered, as was the conclusion in previous subsections.

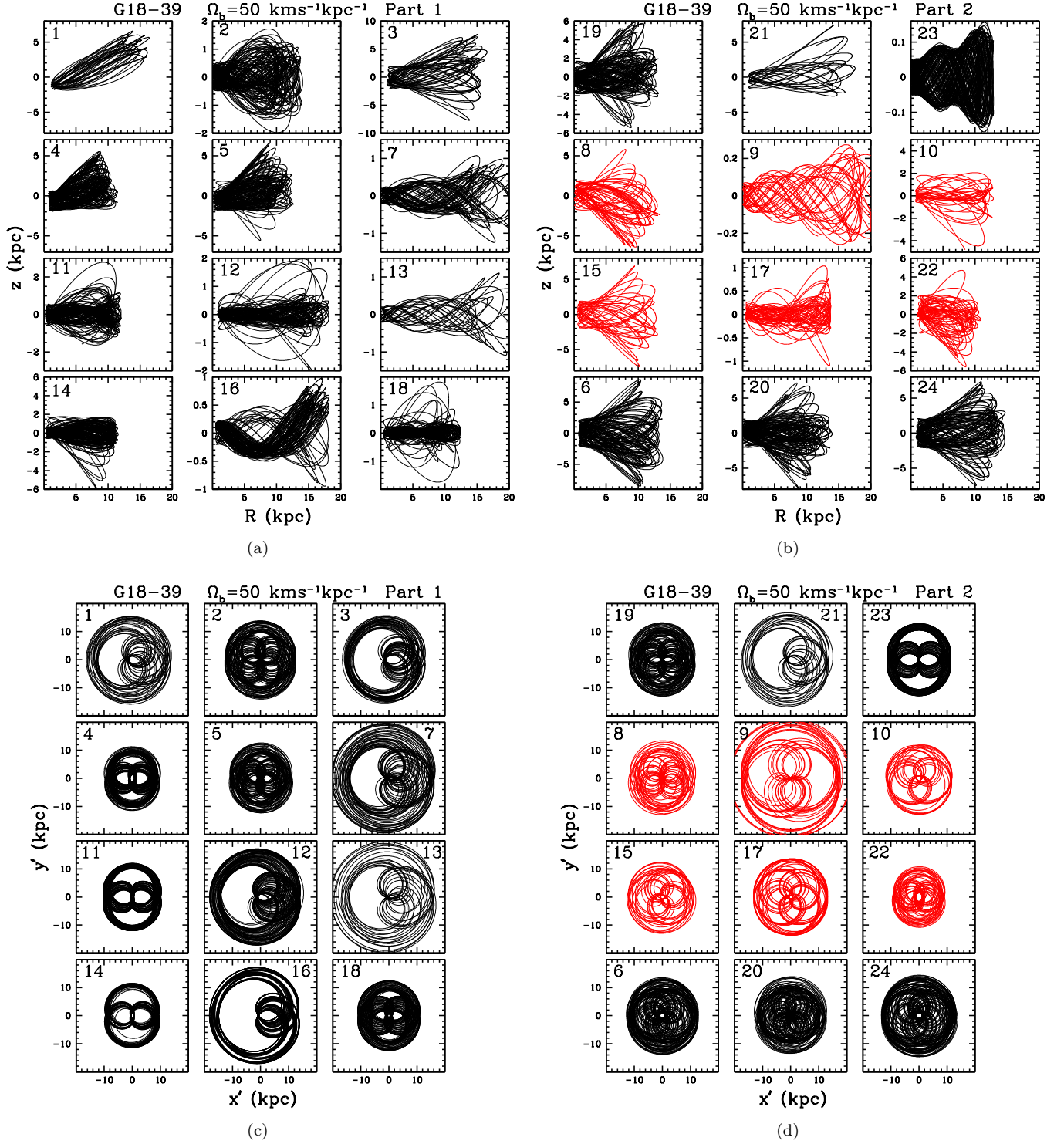


Figure 7. Meridional (frames (a),(b)) and corresponding projected orbits on the Galactic plane in the non-inertial reference frame of the bar (frames (c),(d)), for 24 stars in the group G18-39 with $\Omega_b = 50 \text{ km s}^{-1} \text{ kpc}^{-1}$. The star number is given inside each small frame. The orbits are shown in the trapping intervals of time. The twelve orbits in frames (a),(c) and the three orbits at the top in frames (b),(d) are trapped in an interval of time greater or equal to 5 Gyr. The six orbits in red color in frames (b),(d) are trapped in an interval of time less than 5 Gyr, and the last three in these frames are non-trapped orbits.

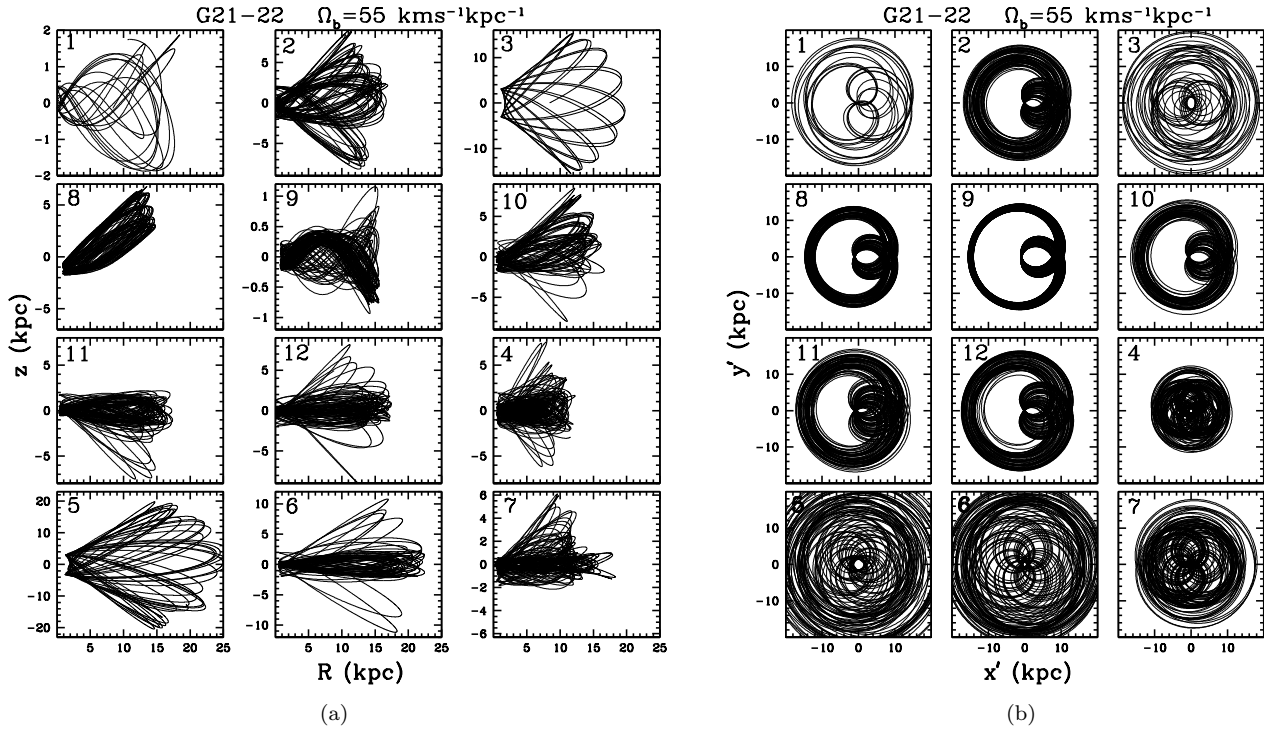


Figure 8. As in Figure 7, for the twelve stars in the group G21-22 with $\Omega_b = 55 \text{ km s}^{-1} \text{ kpc}^{-1}$. The meridional and projected orbits are given in frames (a) and (b), respectively. The first eight stars have trapped orbits in an interval of time greater or equal to 5 Gyr. The last four stars have non-trapped orbits.

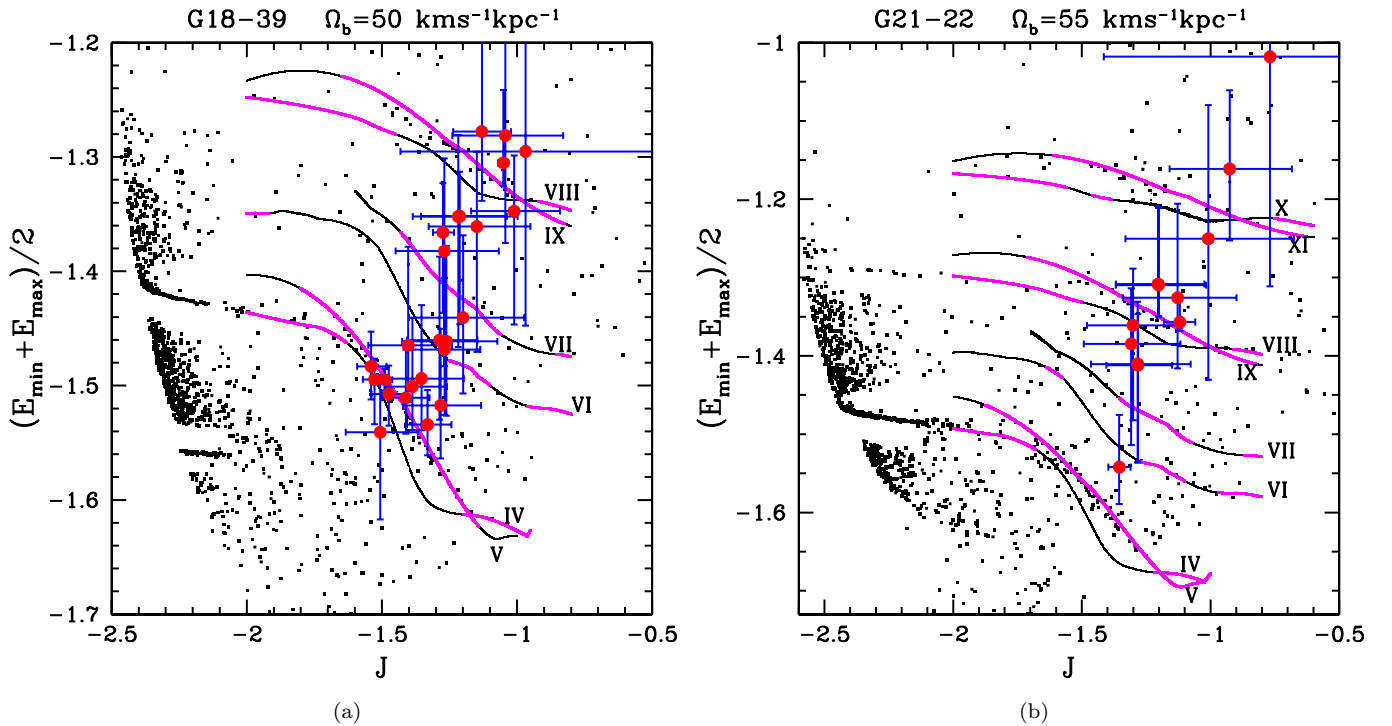


Figure 9. Monte Carlo simulations, (a) in the group G18-39 with $\Omega_b = 50 \text{ km s}^{-1} \text{ kpc}^{-1}$, and (b) in the group G21-22 with $\Omega_b = 55 \text{ km s}^{-1} \text{ kpc}^{-1}$. The red points are the resulting average positions and the blue lines their associated dispersions. Compare with frames (c) and (d) of Figures 1 and 2, respectively.

5.1. The trapped orbits

In the previous section we concluded that the majority of stars in the two groups G18-39 and G21-22 are trapped by the two main resonant families V and IX on the Galactic plane, generated by the Galactic bar. This must be reflected in their velocity field parallel to the Galactic plane observed in the solar neighborhood. In this section the two groups are analyzed in the U' - V' plane, or Bottlinger diagram, with U', V' velocities with respect to the LSR. We compare their observed distribution in this plane with the one that can be inferred from the kinematic properties of their trapping families.

In Figure 10 we give the observed distribution of the two groups in the Bottlinger diagram, obtained with the updated kinematic parameters listed in Table 1. The colors used to differentiate the groups are the same as in figure 7 in the original analysis of the groups made by Silva et al. (2012). Red color for the group G18-39, with a double structure in the U' velocity, and green color for G21-22, only appearing at U' positive, shifted slightly to the right of the G18-39 structure on this side.

To model the distributions shown in Figure 10 we analyze the velocity field U', V' in the solar neighborhood generated by the two main trapping families V and IX. The following procedure is considered: to illustrate the method, we focus on the results shown in frames (c) and (d) of Figures 1 and 2, respectively; i.e., the cases $\Omega_b = 50 \text{ km s}^{-1} \text{ kpc}^{-1}$ in the group G18-39, and $\Omega_b = 55 \text{ km s}^{-1} \text{ kpc}^{-1}$ in the group G21-22. In these two cases, the star orbits in both groups trapped by families V and IX lie in some known different intervals in J , the Jacobi constant. Taking a fine grid in J , 2D periodic orbits of a trapping family lying in each of these intervals are computed. Also, some different 2D tube orbits around these periodic orbits are computed during several revolutions around the Galactic center. Tube orbits have already been employed in the extended Poincaré diagrams shown in Figures 4 and 5. In those figures we saw that a 3D trapped orbit approximately distributes among the tube orbits; thus, we expect that the 2D velocity field produced by tube orbits reflects on the observed distribution of U', V' velocities of 3D trapped star orbits. To proceed with the analysis, a radius of 500 pc is considered for the solar vicinity, which is an appropriate value according to the distances given in Table 1 for the stars in both groups. Next, with a given *present* position angle of the major axis of the Galactic bar and the Sun's galactocentric distance R_0 (see Table 2), the solar neighborhood is defined in the non-inertial reference frame where the bar is at rest, in which the 2D periodic and tube orbits are computed. When one of these orbits crosses the solar neighborhood, we take orbital points within this vicinity separated by 100 pc, and in each point transform the velocity to the inertial reference frame; finally, the corresponding U', V' velocities with respect to the LSR are obtained in all these internal points, and a comparison with the observed distributions can be made.

Figure 11 shows the comparisons for the two groups. In frame (a) the black points correspond to the observed distribution in Figure 10 for the group G18-39; the points with a red circle are the stars trapped by family V, and with a blue circle the stars trapped by family IX. The very small red and blue points, which appear approximately as a continuum, correspond respectively to internal orbital points in the solar neighborhood of periodic and tube orbits in families V and IX. There are some gaps in the distribution of these small points because the number of tube orbits around each periodic orbit was small (about 10 orbits). Notice the approximate concordance of the circled red and blue points with the corresponding red and blue regions. There is a blue region at positive U' which is not populated by stars in the group. This region appears again in frame (b), in relation with the group G21-22. In this second frame the black points are the green points in Figure 10. From Table 3, the main trapping family is family IX, with family V not appearing in this case. Again, the trapped points, with a blue circle, lie approximately in a blue region of periodic and tube orbits in family IX. The blue regions here and in frame (a) have almost the same location, the small difference is due to the different values $\Omega_b = 50, 55 \text{ km s}^{-1} \text{ kpc}^{-1}$, respectively. This Figure 11 already points to the observed shift or separation of the groups shown in Figure 10: some stars in the group G18-39 are trapped by family V and lie on its two branches at U' positive and negative; other stars in this group are trapped by family IX and lie on the U' -negative branch of this family. The stars in the group G21-22 are mainly trapped by family IX, lying on its U' -positive branch.

The appearance of two branches, shown in Figure 11, one at U' positive and the other at U' negative, due to periodic and tube orbits in families V and IX, results from the orbital behavior of these families when they cross the solar neighborhood. To illustrate this point, in Figure 12 we show again the tube orbit in family V given in frame (d) of Figure 3. The solar vicinity is shown with a red circle and the major axis of the bar, i.e., the x' -axis, makes an angle of 20° with the Sun-Galactic center line. Due to ordered motion of tube orbits, in the U' velocity the orbit has positive and negative values in somewhat narrow intervals when it crosses the solar vicinity. Different tube orbits will have different intervals, thus their superposition will enlarge the total range of values. A similar figure can be done

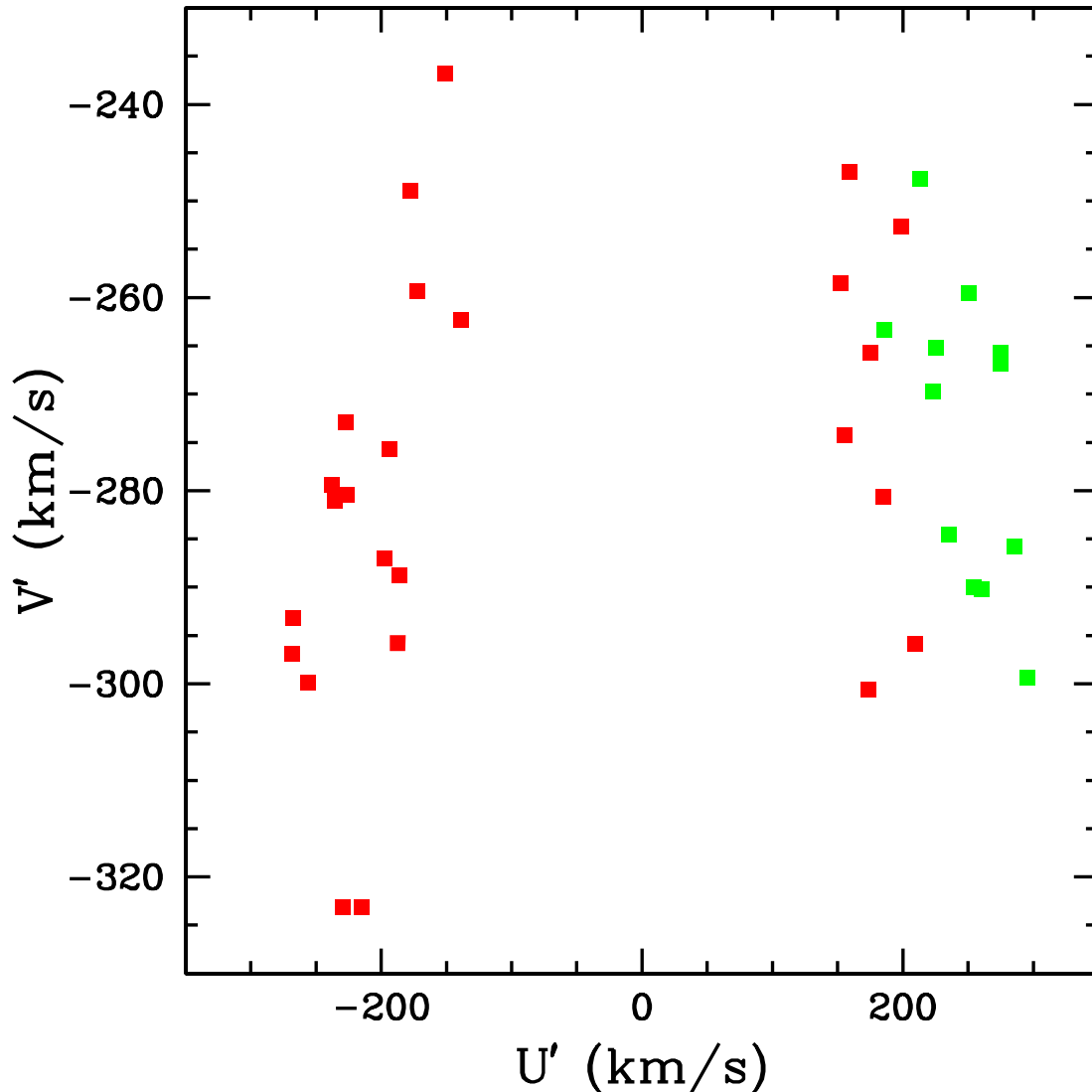


Figure 10. The two groups in the Bottlinger diagram, with U', V' observed velocities with respect to the LSR. The red points correspond to G18-39 and the green points to G21-22.

for family IX, taking for example a tube orbit with the form of the projected orbit of star number 10 in frame (b) of Figure 8. The position of the two branches in each family in the Bottlinger diagram will be different.

To compare with the joint observed distribution in Figure 10, in Figure 13 we show together the two groups G18-39 and G21-22 under the two different values $\Omega_b = 50, 55 \text{ km s}^{-1} \text{ kpc}^{-1}$. In both frames (a) and (b) the black points correspond to the group G18-39 and the green points to the group G21-22. Points circled in red are stars trapped by family V, and those circled in blue are stars trapped by family IX. We note that with $\Omega_b = 50 \text{ km s}^{-1} \text{ kpc}^{-1}$ there are more stars trapped by family V than with the higher value $\Omega_b = 55 \text{ km s}^{-1} \text{ kpc}^{-1}$, and conversely, the number of stars trapped by family IX increases with the higher value of Ω_b (see Table 3). Also, the red-circled and blue-circled points lie approximately in the corresponding red and blue regions produced by families V and IX, respectively; thus showing the observed shift in Figure 10.

5.2. The non-trapped orbits

In the last section the U', V' velocities in the solar neighborhood of trapped 3D orbits in the two groups G18-39 and G21-22 have been modeled through the 2D velocity fields of periodic and tube orbits in the resonant families V and IX on the Galactic plane. Of the uncircled points in Figures 11 and 13, several correspond to non-trapped orbits, but lie on or near the regions of families V and IX; the rest correspond to orbits trapped by other families.

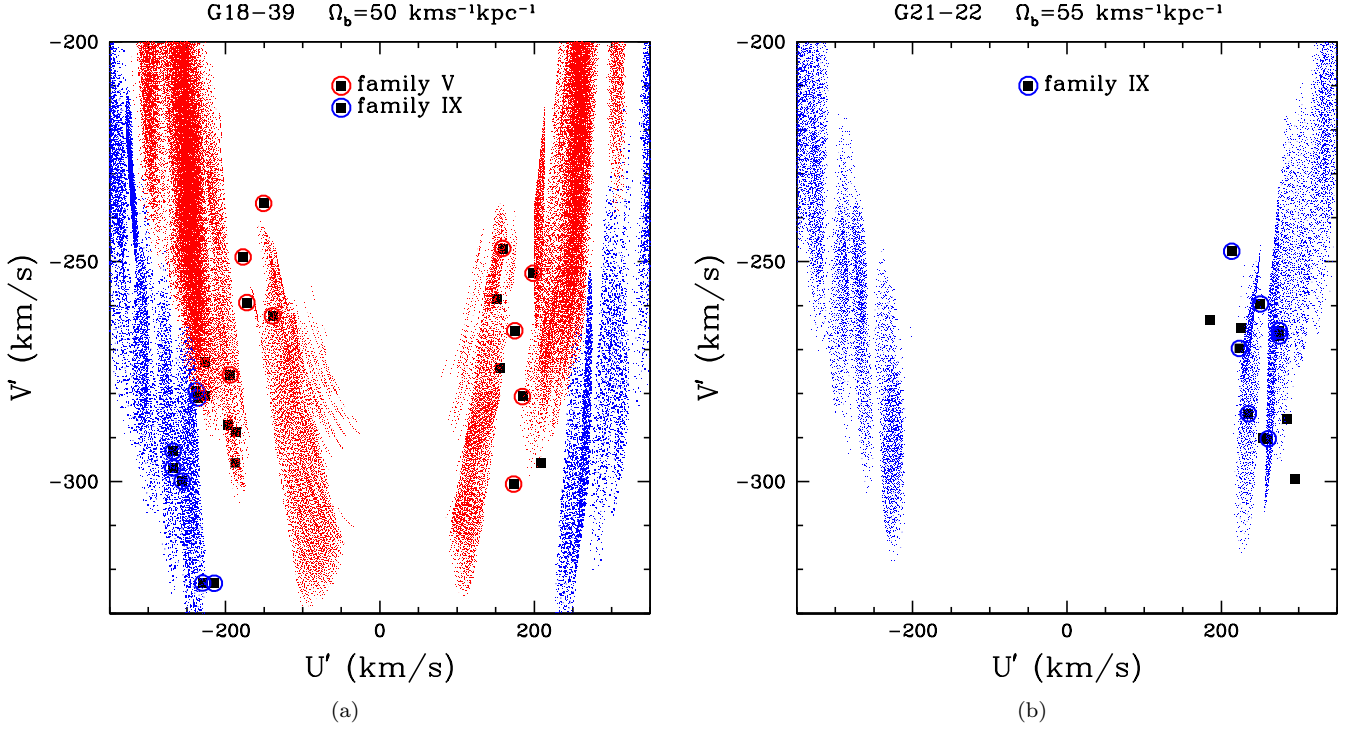


Figure 11. The observed and inferred distributions in the Bottlinger diagram for the group G18-39 with $\Omega_b = 50 \text{ km s}^{-1} \text{ kpc}^{-1}$ (frame (a)), and the group G21-22 with $\Omega_b = 55 \text{ km s}^{-1} \text{ kpc}^{-1}$ (frame (b)). In (a) the black points correspond to the observed distribution in Figure 10 for the group G18-39. The points with a red circle are the stars trapped by family V, and those with a blue circle are stars trapped by family IX. The red and blue regions show values for internal orbital points in the solar neighborhood of periodic and tube orbits in families V and IX, respectively. There is an approximate concordance of the circled red and blue points with the corresponding red and blue regions. In (b) the black points are the observed green points in Figure 10 for the group G21-22. The points with a blue circle are orbits trapped by family IX. The blue regions correspond to periodic and tube orbits in family IX.

For trapped orbits, in Section 4.2 we mentioned how the trapping time was determined in a given orbit. In Table 3 we have listed these intervals of time in each case. Most of the trapped orbits have trapping intervals of time equal to the total computed orbital time of 10 Gyr. In Figure 14 we show an example of an orbit which is trapped in a limited interval of time, but at first sight this orbit appears as a non-trapped orbit. This Figure gives the projected orbit, during the total time of 10 Gyr, of star with number 21 in the group G18-39, with $\Omega_b = 50 \text{ km s}^{-1} \text{ kpc}^{-1}$. There is an interval of time (5 Gyr), listed in Table 3, where the orbit is trapped by family IX; see this part of the orbit in the first row in frame (d) of Figure 7. In this interval of time, which includes the present time, the orbit keeps its form fixed in the non-inertial frame, and outside this interval this form attains a precession-like motion around the z' axis, like in a rosette orbit, almost with no significant variation of its radial and azimuthal motions in the inner Galactic region; this is only approximate, due to the non-axisymmetry of the potential. This means that the orbital U', V' velocity field within the solar vicinity will remain approximately the same at later times, when the projected orbit crosses this vicinity again, as that presented at the initial trapping time interval. For non-trapped orbits close to a trapping region the precession-like motion will be the dominant orbital behavior, and it is expected that their points in the Bottlinger diagram when the orbit is inside the solar vicinity will lie close to the trapped orbits.

To analyze this last point, for non-trapped orbits we calculate the 3D orbit during 10 Gyr and determine the U', V' velocities in orbital points whose *projected* positions on the non-inertial x', y' Galactic plane lie within the solar vicinity. As an example, we consider the four non-trapped orbits in the group G18-39 with $\Omega_b = 50 \text{ km s}^{-1} \text{ kpc}^{-1}$, as shown in Table 3. These orbits correspond to stars with numbers 6, 20, 24, 25 in this group. The last rows in frames (b) and (d) of Figure 7 show the meridional and projected orbits for three of these stars. Their points in the Bottlinger diagram are four of the uncircled points in frame (a) of Figure 11. The resulting U', V' velocities for these four non-trapped orbits are shown in Figure 15. Each present point is marked with a colored big circled square, and some lines with the same color define other velocities in projected positions within the solar vicinity. These lines lie approximately near the red and blue regions produced by families V and IX in frame (a) of Figure 11. Thus, it appears that these

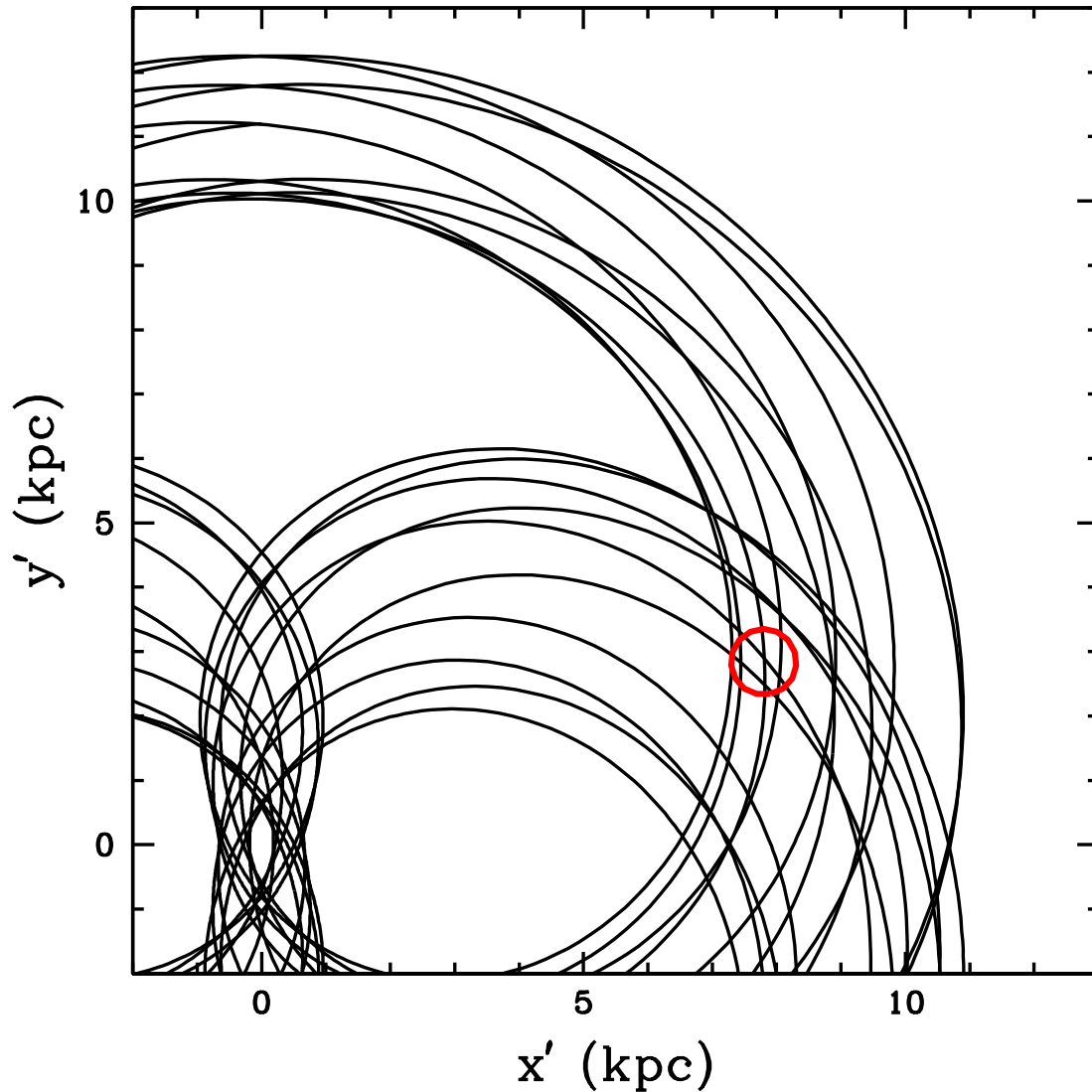


Figure 12. This figure illustrates the appearance of two branches in the Bottlinger diagram, at U' positive and U' negative as shown in Figure 11, of periodic and tube orbits in families V and IX. As an example, the tube orbit in family V given in frame (d) of Figure 3 is plotted. The solar vicinity is shown with a red circle at 20° with the x' -axis, the major axis of the bar. When the orbit crosses the solar vicinity the U' velocity has positive and negative values within narrow intervals, due to ordered motion of the tube orbit. A similar figure can be done for family IX.

four non-trapped orbits could be nearly trapped by these families. However, there are four other uncircled points in that frame (a) of Figure 11 which also lie near the red and blue regions but are trapped by other families in limited intervals of time, as shown in Table 3. Thus, in the considered solar neighborhood several resonant families coexist, and giving a point in the Bottlinger diagram is not sufficient to determine a possible trapping family. The spatial position within the 3D solar neighborhood is also necessary, apart from the open problem pointed out in subsection 4.2 of finding general conditions for a 3D orbit to be trapped by a 2D resonance on the Galactic plane. The value of Ω_b is very important in the resulting trapping family; as can be seen in Figures 1 and 2 a given orbit may or may not be trapped depending on the value of Ω_b . In conclusion, we are only confident with the majority of stars in both groups G18-39 and G21-22 which have been shown to be trapped by families V and IX, taking Ω_b approximately in the interval $45\text{--}60 \text{ km s}^{-1} \text{ kpc}^{-1}$; other stars in these groups could also be nearly trapped by these families or are trapped by other less important resonant families.

6. CONCLUSIONS

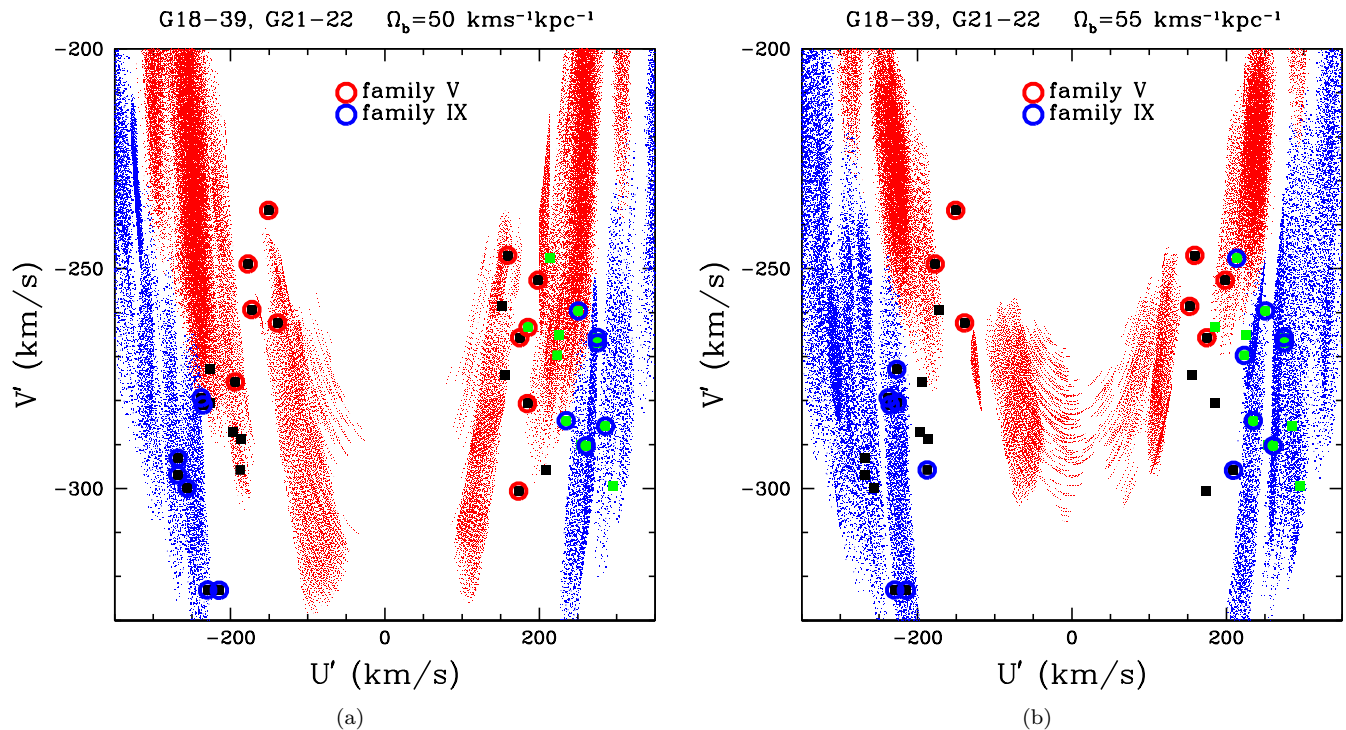


Figure 13. The two groups G18-39 and G21-22 in the Bottlinger diagram with $\Omega_b = 50 \text{ km s}^{-1} \text{ kpc}^{-1}$ (frame (a)), and $\Omega_b = 55 \text{ km s}^{-1} \text{ kpc}^{-1}$ (frame (b)). The black points correspond to the group G18-39 and the green points to the group G21-22. Points circled in red are stars trapped by family V, and those circled in blue are stars trapped by family IX. All these circled points lie approximately in the corresponding red and blue regions produced by families V and IX, respectively. In frame (b) the number of stars trapped by family V and family IX is respectively less and greater than in frame (a).

The star groups G18-39 and G21-22 pertaining to the Galactic halo, and at the present time within the solar neighborhood, were originally identified by [Silva et al. \(2012\)](#). The 3D orbits of these two groups have been computed in a Galactic potential including a Galactic bar, and have been analyzed in terms of the orbital structure of resonant orbits on the Galactic plane created by the bar component. In a previous study ([Moreno et al. 2015](#)) we have seen how 3D star orbits can be trapped by 2D resonant families due to the Galactic bar. In the present analysis we have shown that the majority of stars in both groups G18-39 and G21-22 are indeed trapped, mainly by the two resonant families V and IX studied in [Moreno et al. \(2015\)](#), taking Ω_b approximately in the interval $45\text{--}60 \text{ km s}^{-1} \text{ kpc}^{-1}$.

An explanation of the kinematics presented by the stars in these groups was given by [Silva et al. \(2012\)](#). They proposed that the observed LSR U–V velocity field may be related to the results of simulations made by [Meza et al. \(2005\)](#) for the accretion of a dwarf galaxy by our own Galaxy. Those simulations may give a double-peaked U' velocity distribution of stripped stars from the dwarf galaxy, as observed in particular in the group G18-39. The results that we obtain with our orbital computations give an alternative explanation of the kinematics in both groups G18-39 and G21-22, which has to do closely with the structure of resonant families existing in the non-axisymmetric potential of our Galaxy. We have shown that the observed LSR U–V velocity field of the stars in these groups can be naturally explained as a result of their trapping by resonant families on the Galactic plane generated by the Galactic bar, mainly families V and IX. This analysis may help to understand the identification of other known star groups as the possible result of the interactions produced by resonances on stars close to resonant families. For the two groups G18-39 and G21-22 we conclude that the majority of their stars are members of the supergroups of stars in the Galaxy trapped by the resonant families V and IX.

Acknowledgements

We wish to thank greatly Benjamín Hernández for his help and support from the Universidad Nacional Autónoma de México, grant DGAPA PAPIIT IN 100918. E.M acknowledge support from UNAM/PAPIIT grant IN105916 and IN 114114. J.G.F-T is supported by FONDECYT No. 3180210 and the Chilean BASAL Centro de Excelencia en

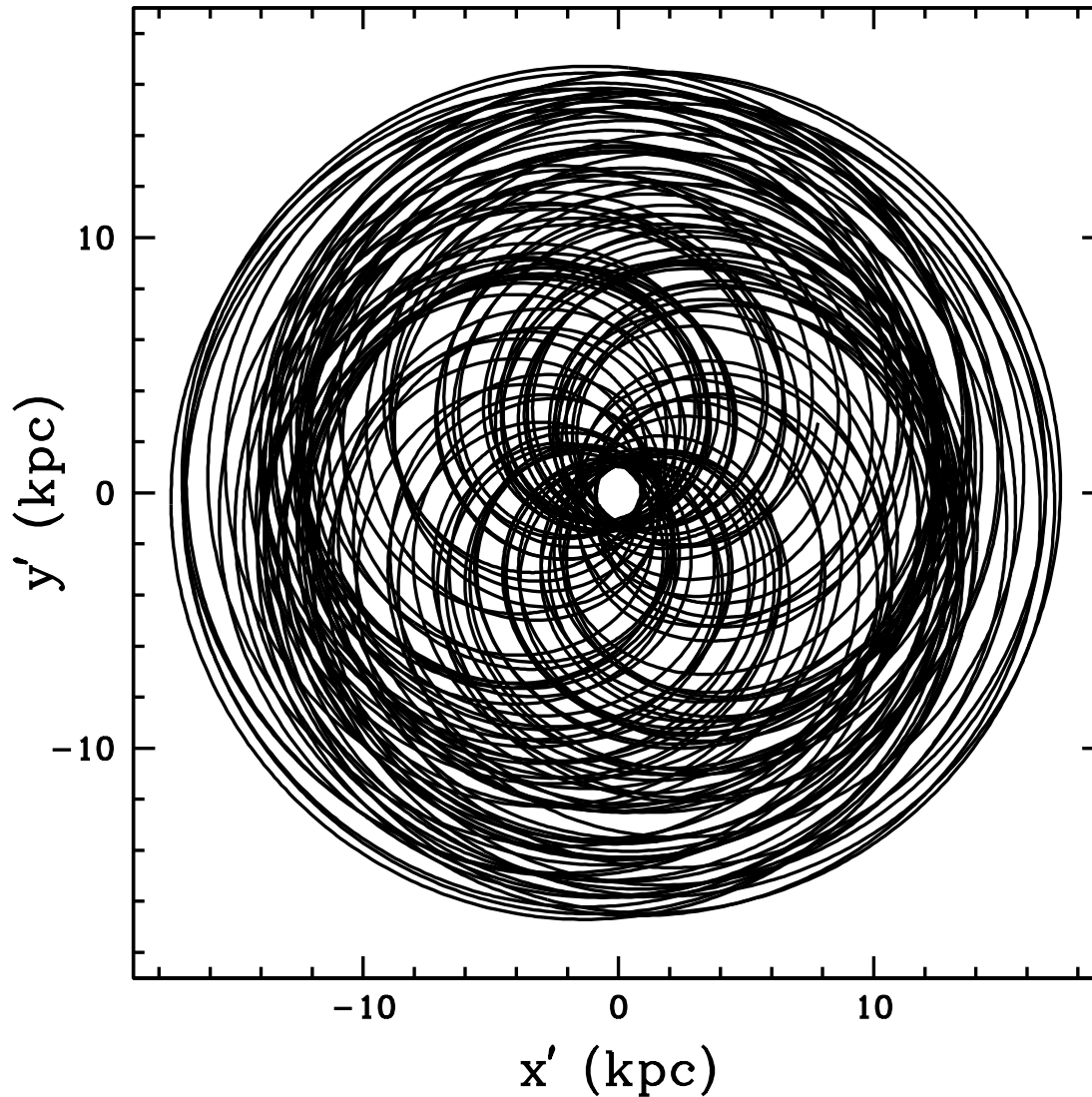


Figure 14. This is the projected orbit during the total time of 10 Gyr of star with number 21 in the group G18-39, with $\Omega_b = 50 \text{ km s}^{-1} \text{ kpc}^{-1}$. In an interval of time of 5 Gyr, listed in Table 3, the orbit is trapped by family IX. See first row in frame (d) of Figure 7 for the projected orbit in this interval.

Astrofísica y Tecnologías Afines (CATA) grant PFB-06/2007.

REFERENCES

- Abolfathi, B., Aguado, D. S., Aguilar, G., et al. 2017, arXiv:1707.09322
- Allen, C., & Santillan, A. 1991, *Revista Mexicana de Astronomía y Astrofísica*, 22, 255
- Antoja, T., Figueras, F., Romero-Gómez, M., et al. 2011, *MNRAS*, 418, 1423
- Antoja, T., Valenzuela, O., Figueras, F., Pichardo, B., & Moreno, E. 2010, *Highlights of Astronomy*, 15, 192
- Antoja, T., Valenzuela, O., Pichardo, B., et al. 2009b, *ApJL*, 700, L78
- Antoja, T., Figueras, F., Pichardo, B., et al. 2009a, *The Galaxy Disk in Cosmological Context*, 254, 4
- Brunthaler, A., Reid, M. J., Menten, K. M., et al. 2011, *Astronomische Nachrichten*, 332, 461
- Contopoulos, G. 2002, *Order and Chaos in Dynamical Astronomy*, Springer, New York.
- Dehnen, W. 1998, *AJ*, 115, 2384
- Eggen, O. J. 1996, *AJ*, 112, 1595
- Eggen, O. J. 1991, *AJ*, 102, 2028
- Eggen, O. J. 1983b, *AJ*, 88, 642
- Eggen, O. J. 1983a, *AJ*, 88, 190
- Eggen, O. J. 1958b, *MNRAS*, 118, 560
- Eggen, O. J. 1958a, *MNRAS*, 118, 65
- Freudenreich, H. T. 1998, *ApJ*, 492, 495
- Gontcharov, G. A. 2006, *Astronomy Letters*, 32, 759

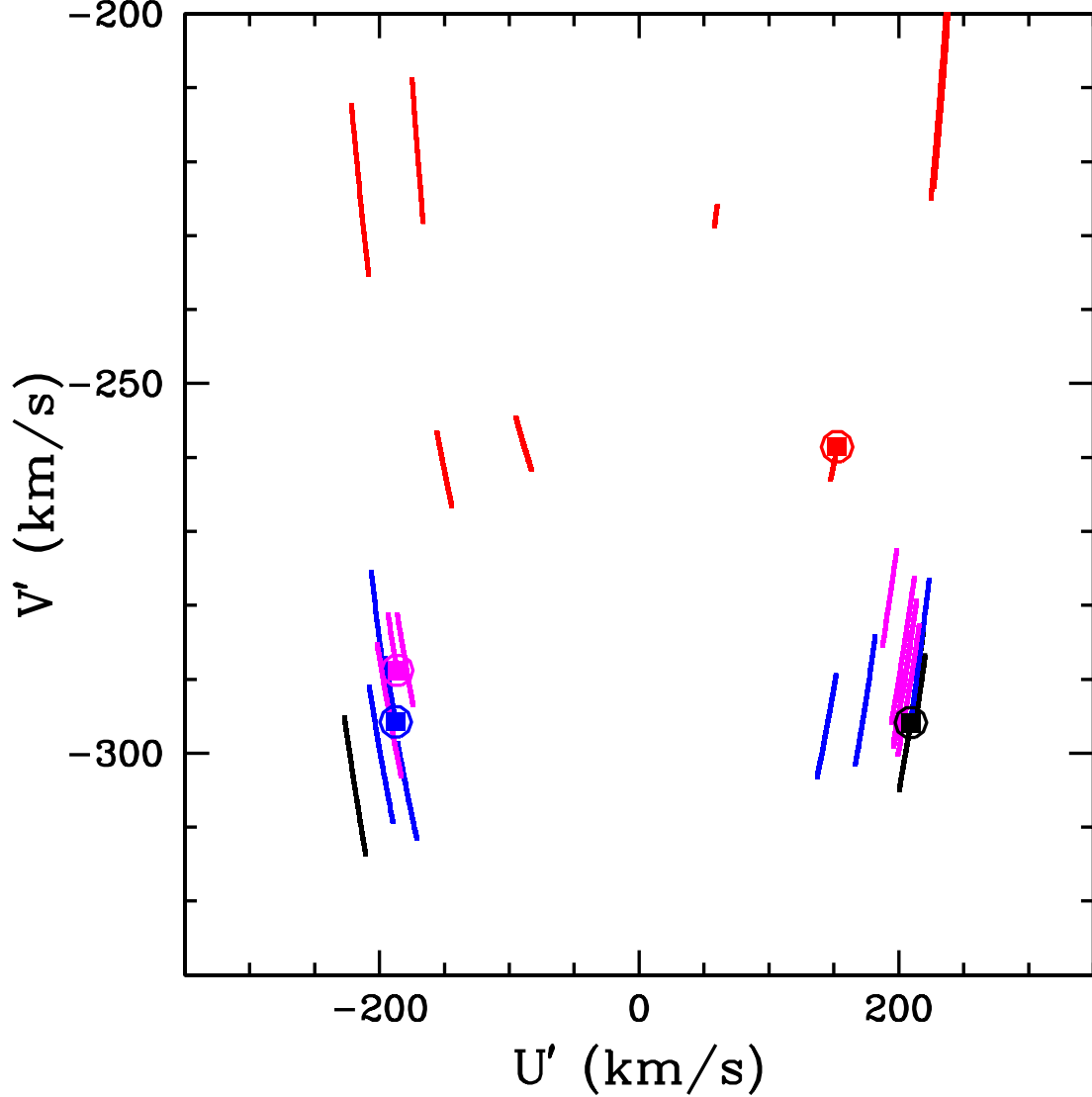


Figure 15. The U', V' velocities for the four non-trapped orbits of stars with numbers 6,20,24,25 in the group G18-39 with $\Omega_b = 50 \text{ km s}^{-1} \text{ kpc}^{-1}$. See Table 3. The colored big circled squares for these stars are four of the uncircled points in frame (a) of Figure 11. The lines with corresponding color define other velocities in projected positions within the solar vicinity. These lines lie approximately in the red and blue regions produced by families V and IX in frame (a) of Figure 11, and these four non-trapped orbits could be nearly trapped by these families.

Helmi, A., White, S. D. M., de Zeeuw, P. T., & Zhao, H. 1999, *Nature*, 402, 53
 Hénon, M. 1965, *Annales d'Astrophysique*, 28, 992
 Hunt, J. A. S., Bovy, J., Pérez-Villegas, A., et al. 2018, *MNRAS*, 474, 95
 Kunder, A., Kordopatis, G., Steinmetz, M., et al. 2017, *AJ*, 153, 75
 Latham, D. W., Stefanik, R. P., Torres, G., et al. 2002, *AJ*, 124, 1144
 Meza, A., Navarro, J. F., Abadi, M. G., & Steinmetz, M. 2005, *MNRAS*, 359, 93
 Moreno, E., Pichardo, B., & Schuster, W. J. 2015, *MNRAS*, 451, 705
 Navarrete, C., Chanamé, J., Ramírez, I., et al. 2015, *ApJ*, 808, 103
 Nissen, P. E., & Schuster, W. J. 2010, *A&A*, 511, L10
 Olano, C. A. 2016, *MNRAS*, 458, 4354

Olano, C. A. 2015, *MNRAS*, 447, 3016
 Pérez-Villegas, A., Portail, M., Wegg, C., & Gerhard, O. 2017, *ApJL*, 840, L2
 Pichardo, B., Martos, M., & Moreno, E. 2004, *ApJ*, 609, 144
 Portail, M., Gerhard, O., Wegg, C., & Ness, M. 2017, *MNRAS*, 465, 1621
 Pourbaix, D., Tokovinin, A. A., Batten, A. H., et al. 2004, *A&A*, 424, 727
 Quillen, A. C., & Minchev, I. 2005, *AJ*, 130, 576
 Schönrich, R., Binney, J., & Dehnen, W. 2010, *MNRAS*, 403, 1829
 Siebert, A., Williams, M. E. K., Siviero, A., et al. 2011, *AJ*, 141, 187
 Silva, J. S., Schuster, W. J., & Contreras, M. E. 2012, *Revista Mexicana de Astronomía y Astrofísica*, 48, 109
 Wylie-de Boer, E., Freeman, K., & Williams, M. 2010, *AJ*, 139, 636

Zhao, J. K., Zhao, G., Chen, Y. Q., et al. 2014, ApJ, 787, 31
Zwitter, T., Siebert, A., Munari, U., et al. 2008, AJ, 136, 421